Supplement of Atmos. Chem. Phys., 21, 2229–2249, 2021
https://doi.org/10.5194/acp-21-2229-2021-supplement

Supplement of

Insights into particulate matter pollution in the North China Plain during wintertime: local contribution or regional transport?

Jiarui Wu et al.

Correspondence to: Guohui Li (ligh@ieecas.cn)

The supplement provides description about model description, model evaluation, and the calculation of average wind direction during the study episode.

Section S1 Parameterization of the heterogeneous oxidation of SO_2 involving aerosol water

The SO_2 heterogeneous reaction parameterization is used in this study in which the SO_2 oxidation in aerosol water by O_2 catalyzed by Fe^{3+} is limited by mass transfer resistances in the gas-phase and the gas-particle interface.

$$\boldsymbol{S(IV)+\frac{1}{2}O_2 \xrightarrow{Fe^{3+}} S(VI)}$$

When the solution pH is between 5.0 and 7.0, the oxidation reaction is second order in dissolved iron and first order in S(IV) and can be expressed as follows (Seinfeld and Pandis, 2006):

$$\boldsymbol{-\frac{d[S(IV)]}{dt}=1\times10^{-3}[S(IV)] \quad 5.0<pH<6.0}$$

$$\boldsymbol{-\frac{d[S(IV)]}{dt}=1\times10^{-4}[S(IV)] \quad pH\sim7.0}$$

where [S(IV)] is the sulfite (S(IV)) concentration. The measured SO_2 mass accommodation coefficient on aqueous surfaces is around 0.1 (Worsnop et al., 1989). Due to sufficient NH_3 and presence of mineral dust in the atmosphere in northern China, the calculated pH in aerosol water is between 5.0 and 7.0 (Cao et al., 2013). The SO_2 uptake coefficient on aerosol water surface is estimated to be about 10^4–10^5 if the sulfite oxidation is catalyzed by Fe^{3+}. The sulfate heterogeneous formation from SO_2 is therefore parameterized as a first-order irreversible uptake by aerosols, with a reactive uptake coefficient of 0.5×10^{-4}, assuming that there is enough alkalinity to maintain the high iron-catalyzed reaction rate:

$$-\frac{d[SO_2]}{dt} = -(\frac{1}{4}\gamma_{SO_2} \upsilon_{SO_2} A_W)[SO_2]$$

where $[SO_2]$ is the SO_2 concentration, A_W is the aerosol water surface area, γ_{SO_2} is the SO_2 reactive uptake coefficient, and υ_{SO_2} is the SO_2 thermal velocity. The aerosol hygroscopic growth is directly predicted by ISORROPIA (Version 1.7) in the model, and the aerosol water surface area is scaled from the calculated wet aerosol surface area using the third-moment of aerosol species.

Section S2 Model Evaluation

Section S2.1 Air pollutants simulations in different cities in the NCP

Considering that there are many monitoring sites in the NCP, scatter plots of observed and simulated $PM_{2.5}$, O_3, NO_2, SO_2 and CO concentrations for all sites in Beijing, Tianjin, Hebei, Henan, Shandong, Shanxi, Jiangsu, and Anhui from 05 December 2015 to 04 Janurary 2016 have also been provided in Figures S4 to S8, respectively. Except Anhui, the correlation coefficients between observed and simulated $PM_{2.5}$ concentrations are generally larger than 0.70 (Figure S4). The model also performs well in simulating the O_3 concentration in the NCP, with correlation coefficients generally larger than 0.80 (Figure S5). The NO_2 concentration in the NCP is also simulated reasonably, with correlation coefficients generally ranging from 0.70 to 0.80 (Figure S6). Considering that the SO_2 is mainly emitted from point sources, which is more sensitive to meteorological conditions, the model has difficulties in simulating the SO_2 concentration, with correlation coefficients generally less than 0.60 (Figure S7). In addition to Tianjin and Shanxi, the CO concentration is also reasonably reproduced, with correlation coefficient larger than 0.70 (Figure S8).

Section S2.2 Cloud properties

Clouds are one of the most important factors affecting the solar radiation reaching the ground. The daily cloud fraction (CF) used in this study was retrieved from Terra- and Aqua-Moderate Resolution Imaging Spectroradiometer (MODIS) level 2 products. Figure S13 presents the scatter plot of the daily retrieved and simulated CF averaged in the NCP from 05 December 2015 to 31 December 2015. Generally, the simulated daily average CF correlates well with that retrieved, with a correlation coefficient of 0.69. The simulated average CF over the NCP during the episode is 52.8%, lower than the MODIS retrieved 78.4%. Numerical models still have difficulties in representing accurately clouds in terms of microphysical processes, cloud morphologies, occurrence and dissipation. In addition, many uncertainties also significantly impact CF retrievals, such as the satellite's view zenith angle, cloud microphysics assumptions, namely cloud phase, particle size and shape, et al. (An and Wang, 2015; Platnick et al., 2017; Zeng et al., 2012; Li et al., 2014). Therefore, it is still difficult to validate cloud simulations using the satellite cloud products.

Section S3 Calculation of the average wind direction

The wind direction simulated in this study is calculated using the U (the velocity toward east) and V (the velocity toward north) component at a specific grid point over the simulation domain and the average wind direction is calculated based on the average U and V.

References

An, N., and Wang, K. C.: A Comparison of MODIS-Derived Cloud Fraction with Surface Observations at Five SURFRAD Sites, J. Appl. Meteorol. Climatol., 54, 1009-1020, 10.1175/jamc-d-14-0206.1, 2015.

Cao, J., Tie, X., Dabberdt, W. F., Jie, T., Zhao, Z., An, Z., and Shen, Z.: On the potential high acid deposition in north eastern China, J. Geophys. Res.-Atmos., 118, 4834–4846, doi:10.1002/jgrd.50381, 2013.

Grieshop, A. P., Logue, J. M., Donahue, N. M., and Robinson, A. L.: Laboratory investigation of photochemical oxidation of organic aerosol from wood fires 1: measurement and simulation of organic aerosol evolution, Atmos. Chem. Phys., 9, 1263-1277, 2009.

Li, Z., Cribb, M.C., and Chang, F.L.: Validation of MODIS-Retrieved Cloud Fractions Using Whole Sky Imager Measurements at the Three ARM Sites., Fourteenth ARM Science Team Meeting Proceedings, Albuquerque, 2014.

Platnick, S., Meyer, K. G., King, M. D., Wind, G., Amarasinghe, N., Marchant, B., Arnold, G. T., Zhang, Z. B., Hubanks, P. A., Holz, R. E., Yang, P., Ridgway, W. L., and Riedi, J.: The MODIS Cloud Optical and Microphysical Products: Collection 6 Updates and Examples From Terra and Aqua, IEEE Trans. Geosci. Remote Sensing, 55, 502-525, 10.1109/tgrs.2016.2610522, 2017.

Robinson, A. L., Donahue, N.M., Shrivastava, M. K.,Weitkamp, E. A., Sage, A. M., Grieshop, A. P., Lane, T. E., Pandis, S. N., and Pierce, J. R.: Rethinking organic aerosols: semivolatile emissions and photochemical aging, Science, 315, 1259-1262, 2007.

Seinfeld, J. H. and Pandis, S. N.: Atmospheric Chemistry and Physics: From Air Pollution to Climate Change, 2nd Edn., John Wiley & Sons Inc., New York, 2006.

Worsnop, D. R., Zahniser, M. S., Kolb, C. E., Gardner, J. A., Wat- son, L. R., Vandoren, J. M., Jayne, J. T., and Davidovits, P.: Temperature-dependence of mass accommodation of SO_2 and H_2O_2 on aqueous surfaces, J. Phys. Chem., 93, 1159-1172, doi:10.1021/j100340a027, 1989.

Zeng, S., Cornet, C., Parol, F., Riedi, J., and Thieuleux, F.: A better understanding of cloud optical thickness derived from the passive sensors MODIS/AQUA and POLDER/PARASOL in the A-Train constellation, Atmos. Chem. Phys., 12, 11245-11259, 10.5194/acp-12-11245-2012, 2012.

Table S1 SOA yield scenarios using a four-product basis set with saturation concentrations of 1, 10, 100, and 1000 μg m^3 at 298 K.

SOA Precursors	Aerosol Yield* Low-NOx Parameterization				Aerosol Yield High-NOx Parameterization				Molecular Weight
	1	10	100	1000	1	10	100	1000	(g mol^{-1})
ALK4	0.000	0.038	0.000	0.000	0.000	0.075	0.000	0.000	120
ALK5	0.000	0.150	0.000	0.000	0.000	0.300	0.000	0.000	150
OLE1	0.001	0.005	0.038	0.150	0.005	0.009	0.060	0.225	120
OLE2	0.003	0.026	0.083	0.270	0.023	0.044	0.129	0.375	120
ARO1	0.003	0.165	0.300	0.435	0.075	0.225	0.375	0.525	150
ARO2	0.002	0.195	0.300	0.435	0.075	0.300	0.375	0.525	150
CRES	-	-	-	-	-	-	-	-	-
ISOP	0.001	0.023	0.015	0.000	0.009	0.030	0.015	0.000	136
TERP	0.012	0.122	0.201	0.500	0.107	0.092	0.359	0.600	180

*The SOA yields are based on an assumed density of 1.5 g cm^{-3}.

Table S2 Parameters used to treat partitioning of POA emissions.

C^* at 298K (μg m^{-3})	0.01	0.1	1	10	10^2	10^3	10^4	10^5	10^6
Fraction of emissions	0.03	0.06	0.09	0.14	0.18	0.30	0.40	0.50	0.80
Emission Phase (Particle:P;Gas:G)	P	P	P	P	P	P	G	G	G
Molecular Weight (g mol^{-1})	250	250	250	250	250	250	250	250	250
ΔH (kJ mol^{-1}) (Robinson et al., 2007)	112	106	100	94	88	82	76	70	64
ΔH (kJ mol^{-1}) (Grieshop et al., 2009)	77	73	69	65	61	57	54	50	46

Supplement Figure Captions

Figure S1 Model simulation domain and designation of source regions. The black filled circles with number denote the meteorological sites used in this study in the NCP. 1: Beijing; 2: Tianjin; 3: Shijiazhuang; 4: Jinan; 5: Zhengzhou; 6: Hefei; 7: Nanjing.

Figure S2 (a) Geopotential heights and (b) the mean sea level pressures with wind vectors during the study episode from 05 December 2015 to 04 January 2016.

Figure S3 Comparison of observed (black dots) and simulated (solid red lines) diurnal profiles of near-surface (a) pressure, (b) temperature, (c) wind speed, and (d) wind direction averaged at monitoring sites in the NCP from 05 December 2015 to 04 January 2016.

Figure S4 Scatter plot of hourly simulated and observed $PM_{2.5}$ concentration in (a) Beijing, (b) Tianjin, (c) Hebei, (d) Henan, (e) Shandong, (f) Shanxi, (g) Anhui, and (h) Jiangsu during the episode from 05 December 2015 to 04 January 2016.

Figure S5 Scatter plot of hourly simulated and observed O_3 concentration in (a) Beijing, (b) Tianjin, (c) Hebei, (d) Henan, (e) Shandong, (f) Shanxi, (g) Anhui, and (h) Jiangsu during the episode from 05 December 2015 to 04 January 2016.

Figure S6 Scatter plot of hourly simulated and observed NO_2 concentration in (a) Beijing, (b) Tianjin, (c) Hebei, (d) Henan, (e) Shandong, (f) Shanxi, (g) Anhui, and (h) Jiangsu during the episode from 05 December 2015 to 04 January 2016.

Figure S7 Scatter plot of hourly simulated and observed SO_2 concentration in (a) Beijing, (b) Tianjin, (c) Hebei, (d) Henan, (e) Shandong, (f) Shanxi, (g) Anhui, and (h) Jiangsu during the episode from 05 December 2015 to 04 January 2016.

Figure S8 Scatter plot of hourly simulated and observed CO concentration in (a) Beijing, (b) Tianjin, (c) Hebei, (d) Henan, (e) Shandong, (f) Shanxi, (g) Anhui, and (h) Jiangsu during the episode from 05 December 2015 to 04 January 2016.

Figure S9 Pattern comparisons of simulated (color contours) vs. observed (colored circles) near-surface mass concentrations of $PM_{2.5}$ concentration at (a) 00:00 BJT, (b) 04:00 BJT, (c) 08:00 BJT, (d) 12:00 BJT, (e) 16:00 BJT, and (e) 20:00 BJT averaged from 05 December 2015 to 04 January 2016. The black arrows indicate simulated surface winds.

Figure S10 Pattern comparisons of simulated (color contours) vs. observed (colored circles) near-surface mass concentrations of O_3 concentration at (a) 00:00 BJT, (b) 04:00 BJT, (c) 08:00 BJT, (d) 12:00 BJT, (e) 16:00 BJT, and (e) 20:00 BJT averaged from 05 December 2015 to 04 January 2016. The black arrows indicate simulated surface winds.

Figure S11 Pattern comparisons of simulated (color contours) vs. observed (colored circles) near-surface mass concentrations of NO_2 concentration at (a) 00:00 BJT, (b) 04:00 BJT, (c) 08:00 BJT, (d) 12:00 BJT, (e) 16:00 BJT, and (e) 20:00 BJT averaged from 05 December 2015 to 04 January 2016. The black arrows indicate simulated surface winds.

Figure S12 Pattern comparisons of simulated (color contours) vs. observed (colored circles) near-surface mass concentrations of SO_2 concentration at (a) 00:00 BJT, (b) 04:00 BJT, (c) 08:00 BJT, (d) 12:00 BJT, (e) 16:00 BJT, and (e) 20:00 BJT averaged from 05 December 2015 to 04 January 2016. The black arrows indicate simulated surface winds.

Figure S13 Scatter plot of the MODIS retrieved and simulated daily cloud fraction averaged in the NCP from 05 December 2015 to 31 December 2015.

Figure S14 Spatial distribution of average $PM_{2.5}$ contributions from Beijing at (a) 00:00 BJT, (b) 04:00 BJT, (c) 08:00 BJT, (d) 12:00 BJT, (e) 16:00 BJT, and (e) 20:00 BJT averaged from 05 December 2015 to 04 January 2016.

Figure S15 Spatial distribution of average $PM_{2.5}$ contributions from Tianjin at (a) 00:00 BJT, (b) 04:00 BJT, (c) 08:00 BJT, (d) 12:00 BJT, (e) 16:00 BJT, and (e) 20:00 BJT averaged from 05 December 2015 to 04 January 2016.

Figure S16 Spatial distribution of average $PM_{2.5}$ contributions from Hebei at (a) 00:00 BJT, (b) 04:00 BJT, (c) 08:00 BJT, (d) 12:00 BJT, (e) 16:00 BJT, and (e) 20:00 BJT averaged from 05 December 2015 to 04 January 2016.

Figure S17 Spatial distribution of average $PM_{2.5}$ contributions from Henan at (a) 00:00 BJT, (b) 04:00 BJT, (c) 08:00 BJT, (d) 12:00 BJT, (e) 16:00 BJT, and (e) 20:00 BJT averaged from 05 December 2015 to 04 January 2016.

Figure S18 Spatial distribution of average $PM_{2.5}$ contributions from Shandong at (a) 00:00 BJT, (b) 04:00 BJT, (c) 08:00 BJT, (d) 12:00 BJT, (e) 16:00 BJT, and (e) 20:00 BJT averaged from 05 December 2015 to 04 January 2016.

Figure S19 Spatial distribution of average $PM_{2.5}$ contributions from Shanxi at (a) 00:00 BJT, (b) 04:00 BJT, (c) 08:00 BJT, (d) 12:00 BJT, (e) 16:00 BJT, and (e) 20:00 BJT averaged from 05 December 2015 to 04 January 2016.

Figure S20 Vertical profiles of average $PM_{2.5}$ contribution from local (red line) and non-local (black line) emissions in (a) Beijing, (b) Tianjin, (c) Hebei, (d) Henan, (e) Shandong, and (f) Shanxi from 05 December 2015 to 04 January 2016.

Figure S21 Spatial distribution of average near-surface $PM_{2.5}$ contributions from (a) residential, (b) transportation, (c) industry, (d) power, and (e) agriculture emission sectors from 05 December 2015 to 04 January 2016.

Figure S22 Average (a) decrease of surface temperature (TSFC), (b) increase of relative humidity (RH), and (c) percentage decrease of PBLH caused by the BC transported from the south of 32°N, as a function of the near-surface $PM_{2.5}$ concentration in the NCP during daytime from 05 December 2015 to 04 January 2016.

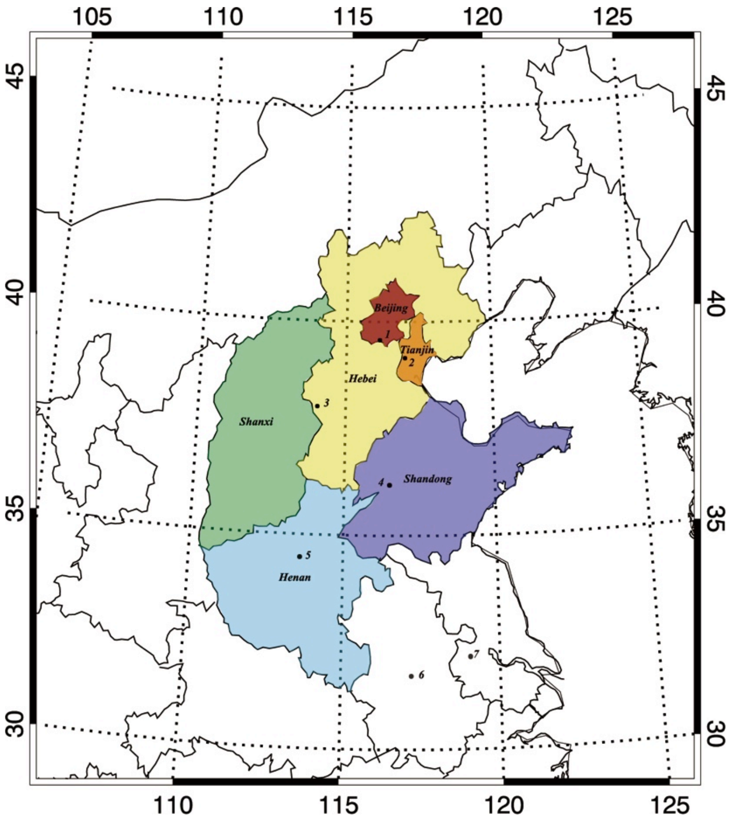

Figure S1 Model simulation domain and designation of source regions. The black filled circles with number denote the meteorological sites used in this study in the NCP. 1: Beijing; 2: Tianjin; 3: Shijiazhuang; 4: Jinan; 5: Zhengzhou; 6: Hefei; 7: Nanjing.

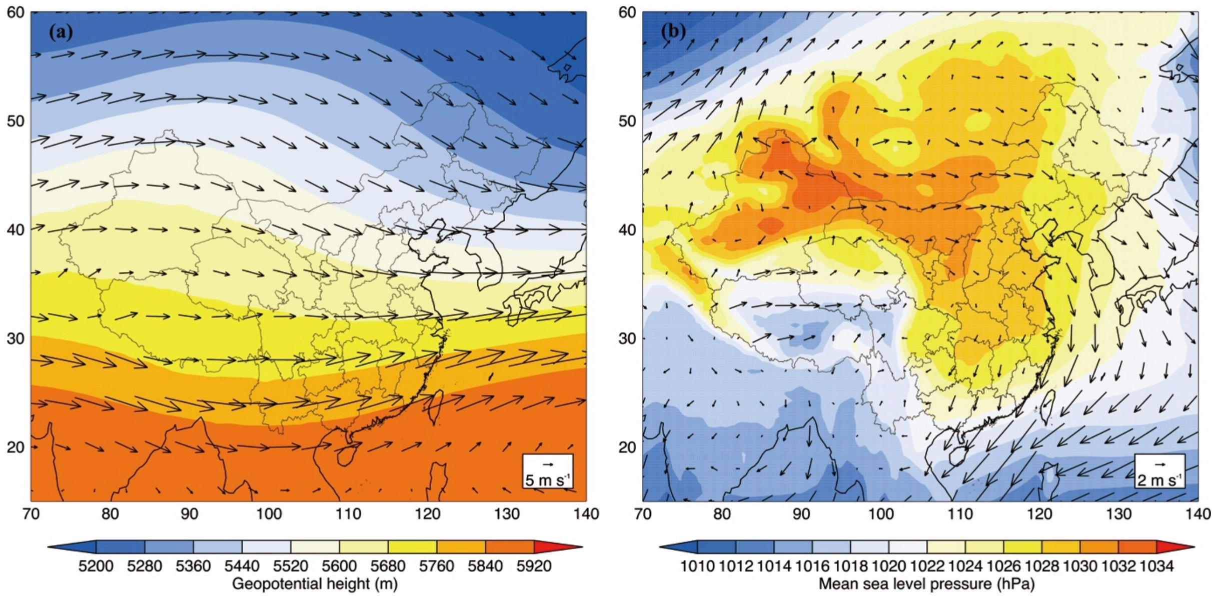

Figure S2 (a) Geopotential heights at 500 hPa and (b) the mean sea level pressures with wind vectors during the study episode from 05 December 2015 to 04 January 2016.

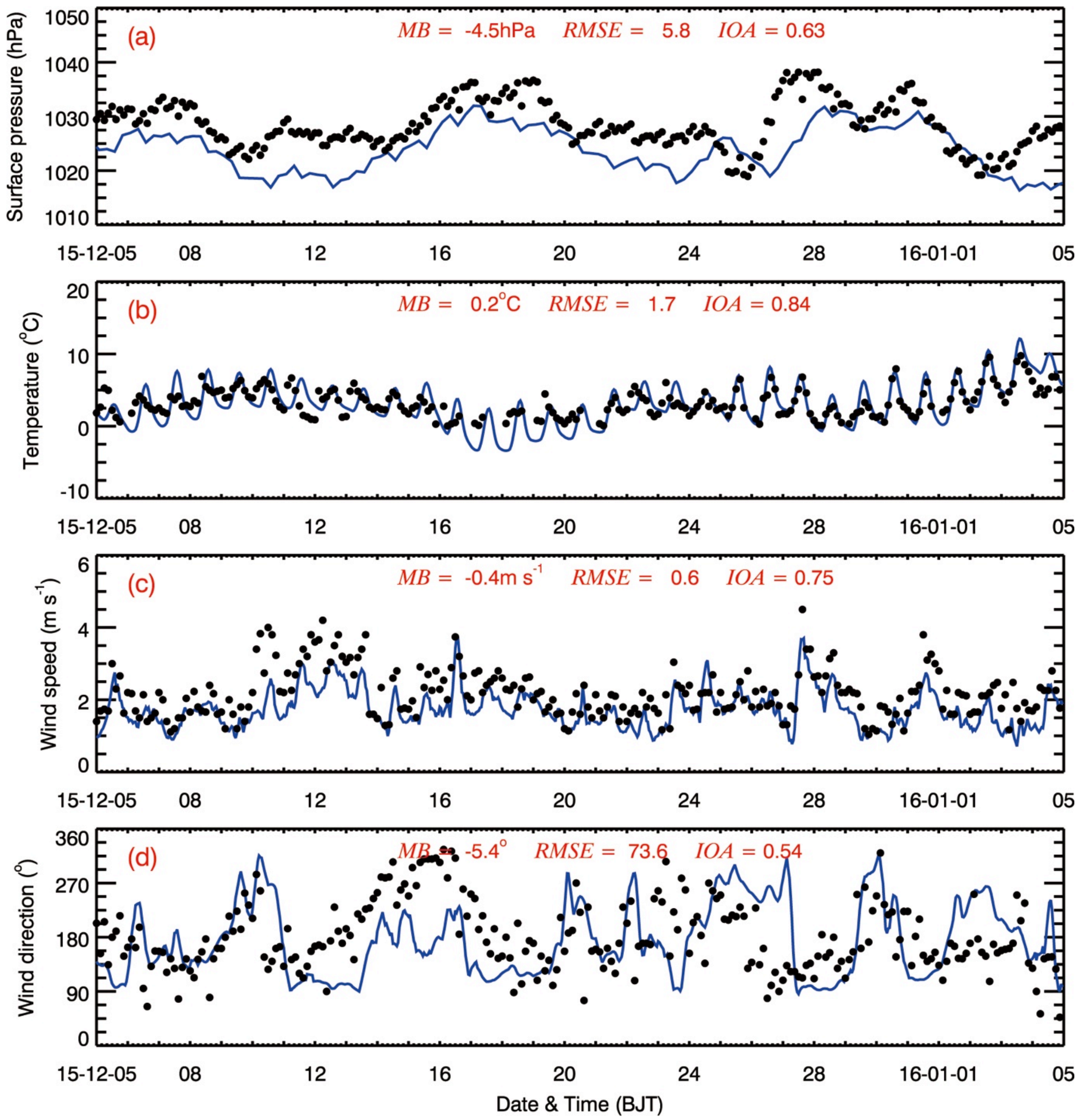

Figure S3 Comparison of observed (black dots) and simulated (solid red lines) diurnal profiles of near-surface (a) pressure, (b) temperature, (c) wind speed, and (d) wind direction averaged at monitoring sites in the NCP from 05 December 2015 to 04 January 2016.

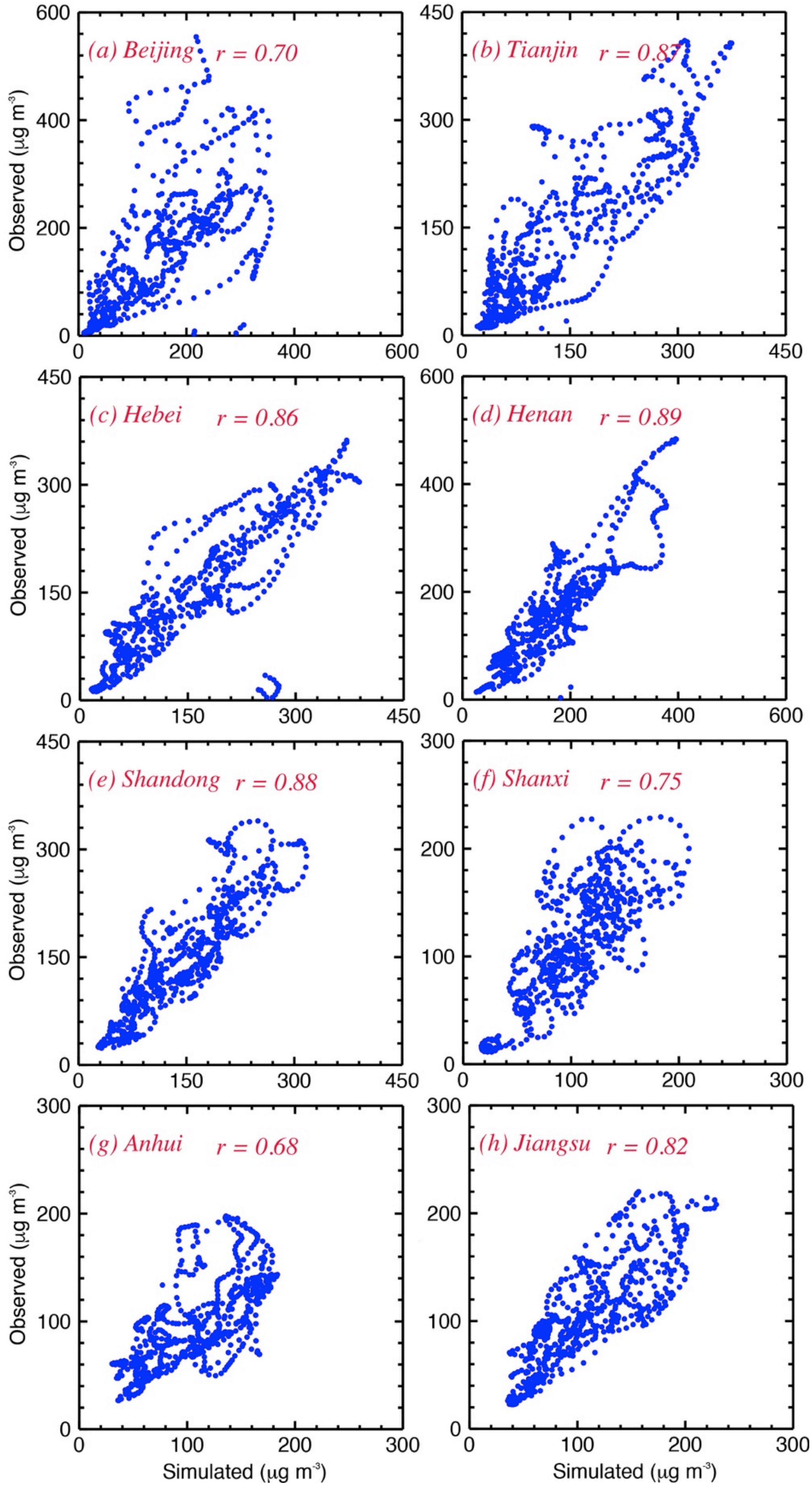

Figure S4 Scatter plot of hourly simulated and observed $PM_{2.5}$ concentration in (a) Beijing, (b) Tianjin, (c) Hebei, (d) Henan, (e) Shandong, (f) Shanxi, (g) Anhui, and (h) Jiangsu during the episode from 05 December 2015 to 04 January 2016.

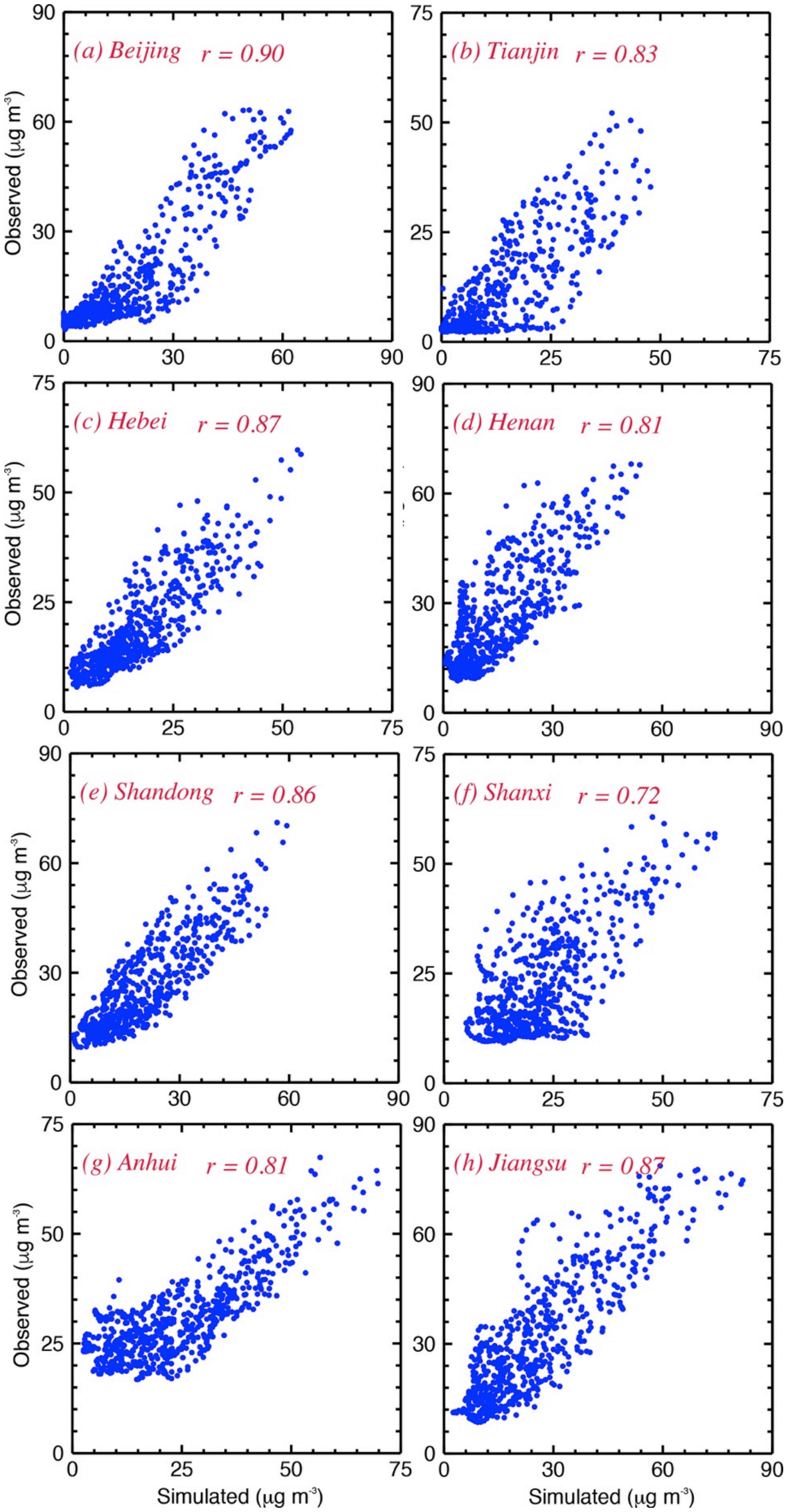

Figure S5 Scatter plot of hourly simulated and observed O_3 concentration in (a) Beijing, (b) Tianjin, (c) Hebei, (d) Henan, (e) Shandong, (f) Shanxi, (g) Anhui, and (h) Jiangsu during the episode from 05 December 2015 to 04 January 2016.

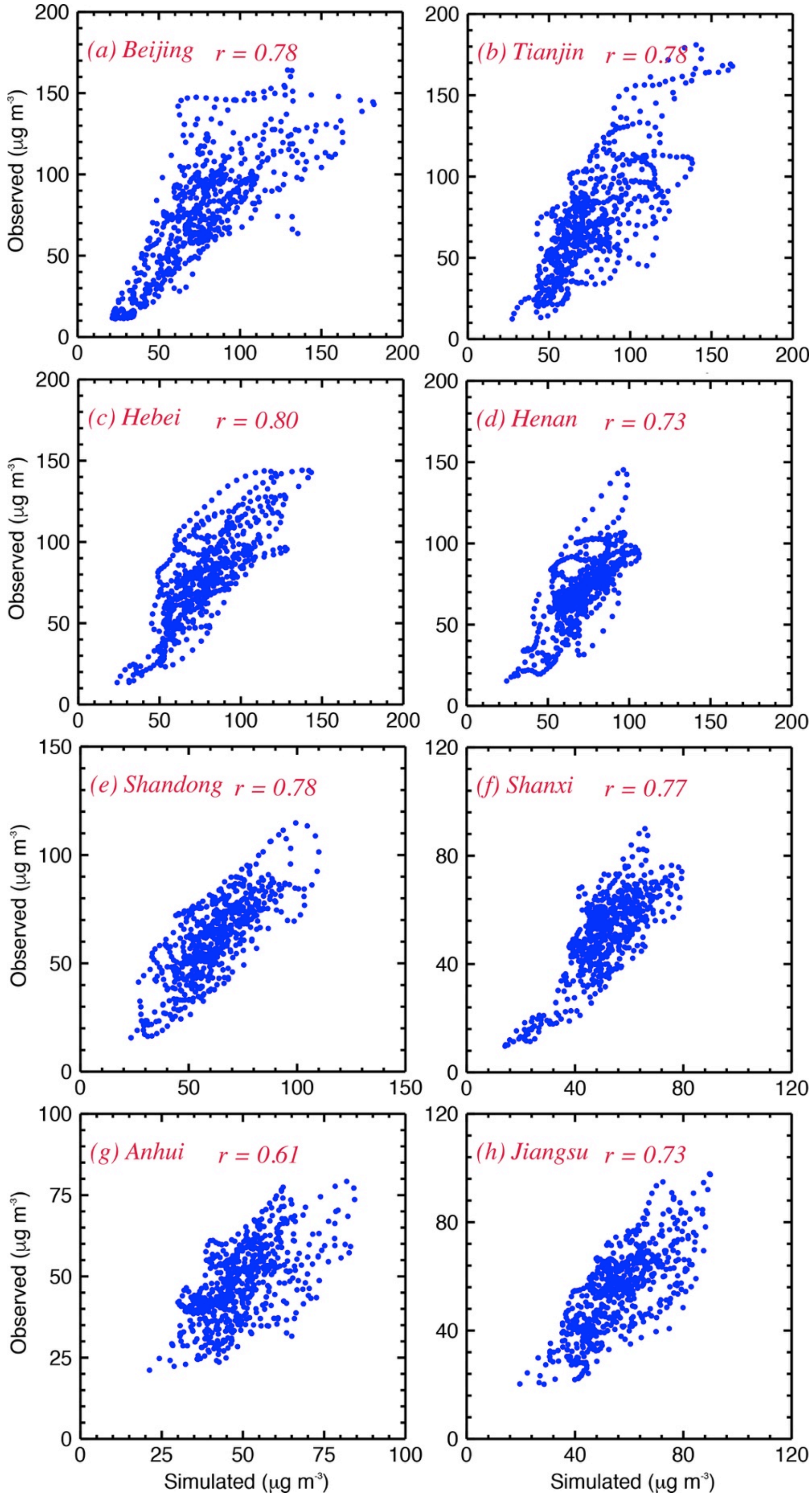

Figure S6 Scatter plot of hourly simulated and observed NO_2 concentration in (a) Beijing, (b) Tianjin, (c) Hebei, (d) Henan, (e) Shandong, (f) Shanxi, (g) Anhui, and (h) Jiangsu during the episode from 05 December 2015 to 04 January 2016.

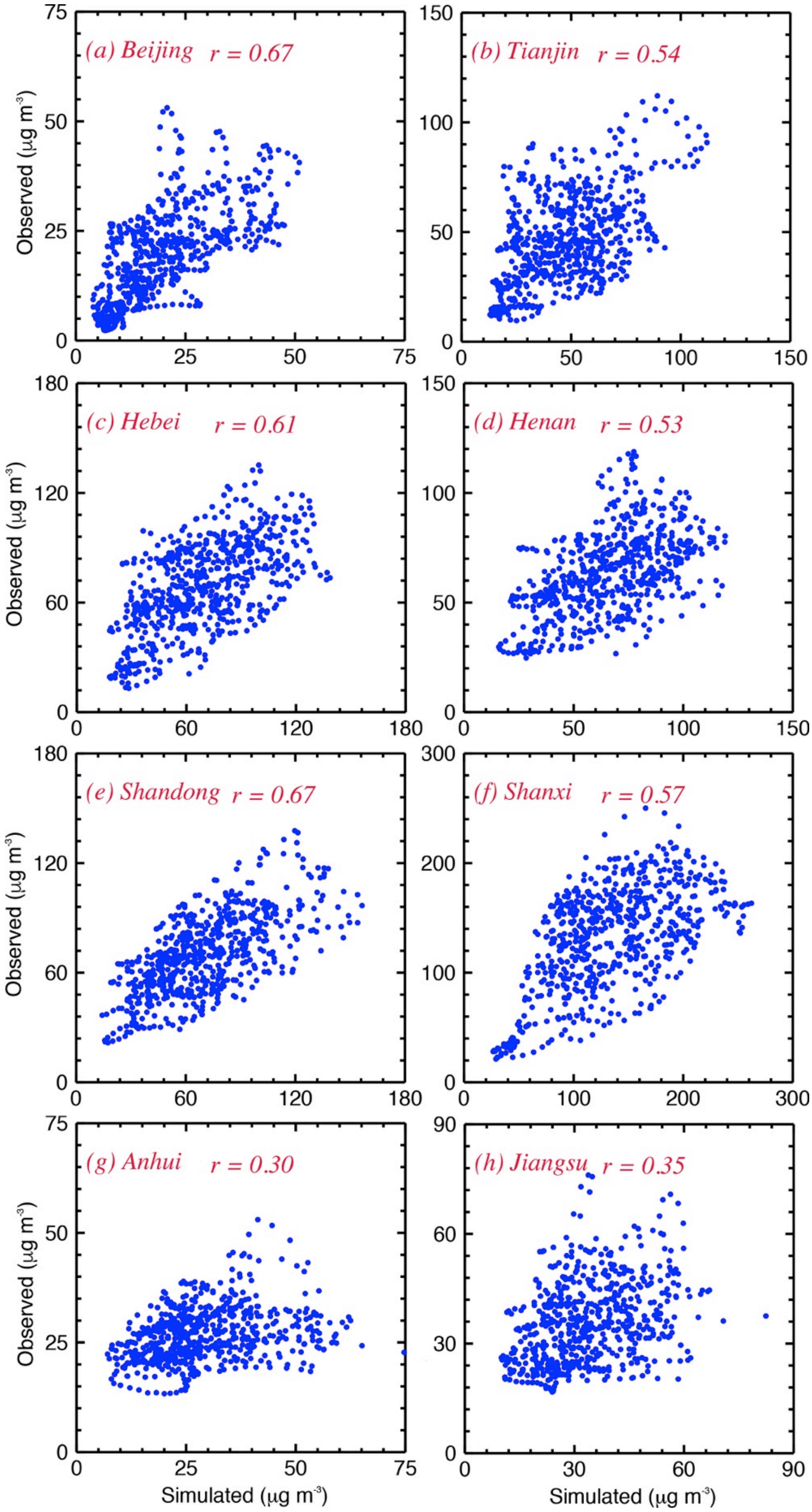

Figure S7 Scatter plot of hourly simulated and observed SO_2 concentration in (a) Beijing, (b) Tianjin, (c) Hebei, (d) Henan, (e) Shandong, (f) Shanxi, (g) Anhui, and (h) Jiangsu during the episode from 05 December 2015 to 04 January 2016.

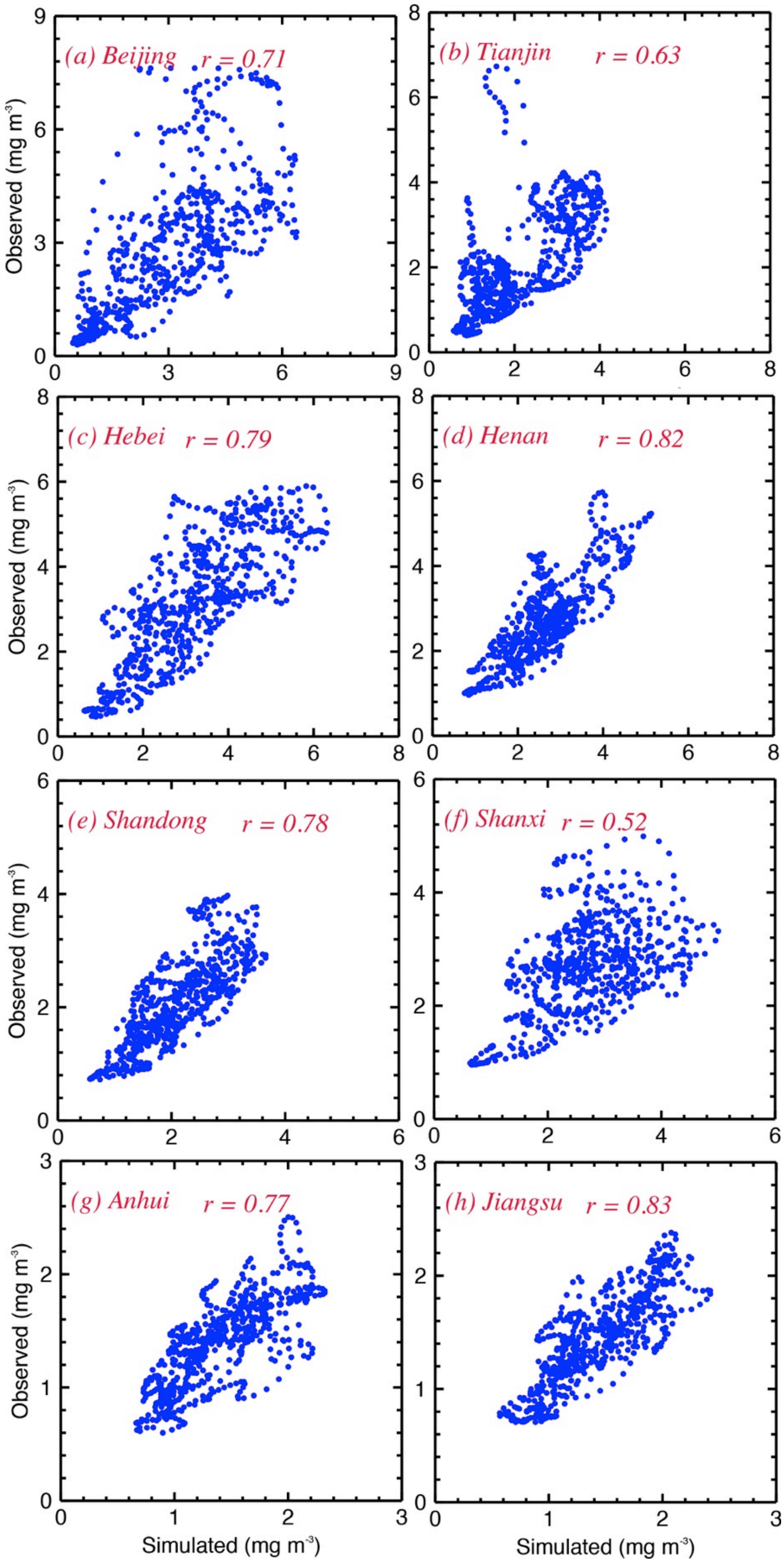

Figure S8 Scatter plot of hourly simulated and observed CO concentration in (a) Beijing, (b) Tianjin, (c) Hebei, (d) Henan, (e) Shandong, (f) Shanxi, (g) Anhui, and (h) Jiangsu during the episode from 05 December 2015 to 04 January 2016.

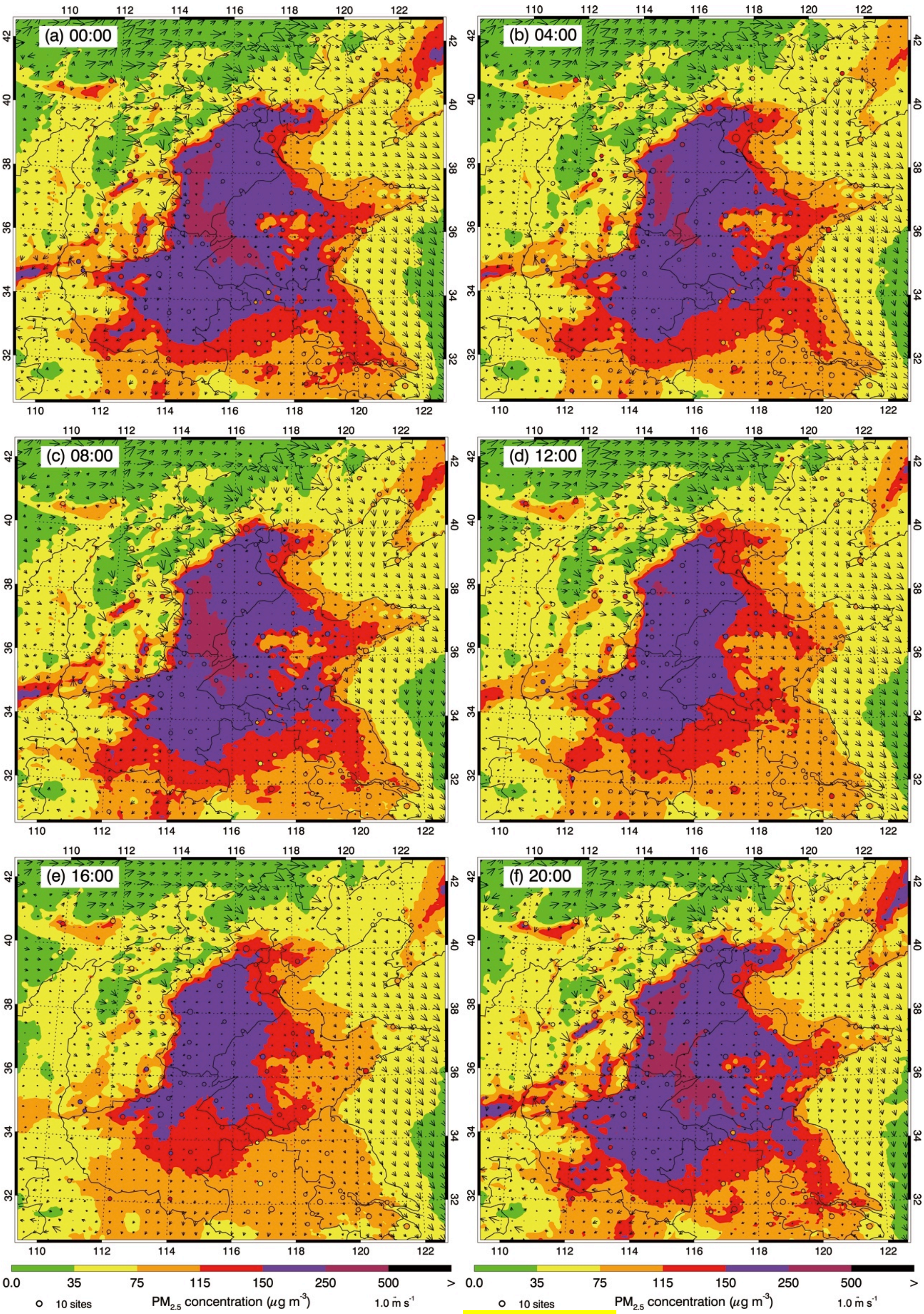

Figure S9 Pattern comparisons of simulated (color contours) vs. observed (colored circles) near-surface mass concentrations of $PM_{2.5}$ concentration at (a) 00:00 BJT, (b) 04:00 BJT, (c) 08:00 BJT, (d) 12:00 BJT, (e) 16:00 BJT, and (e) 20:00 BJT averaged from 05 December 2015 to 04 January 2016. The black arrows indicate simulated surface winds.

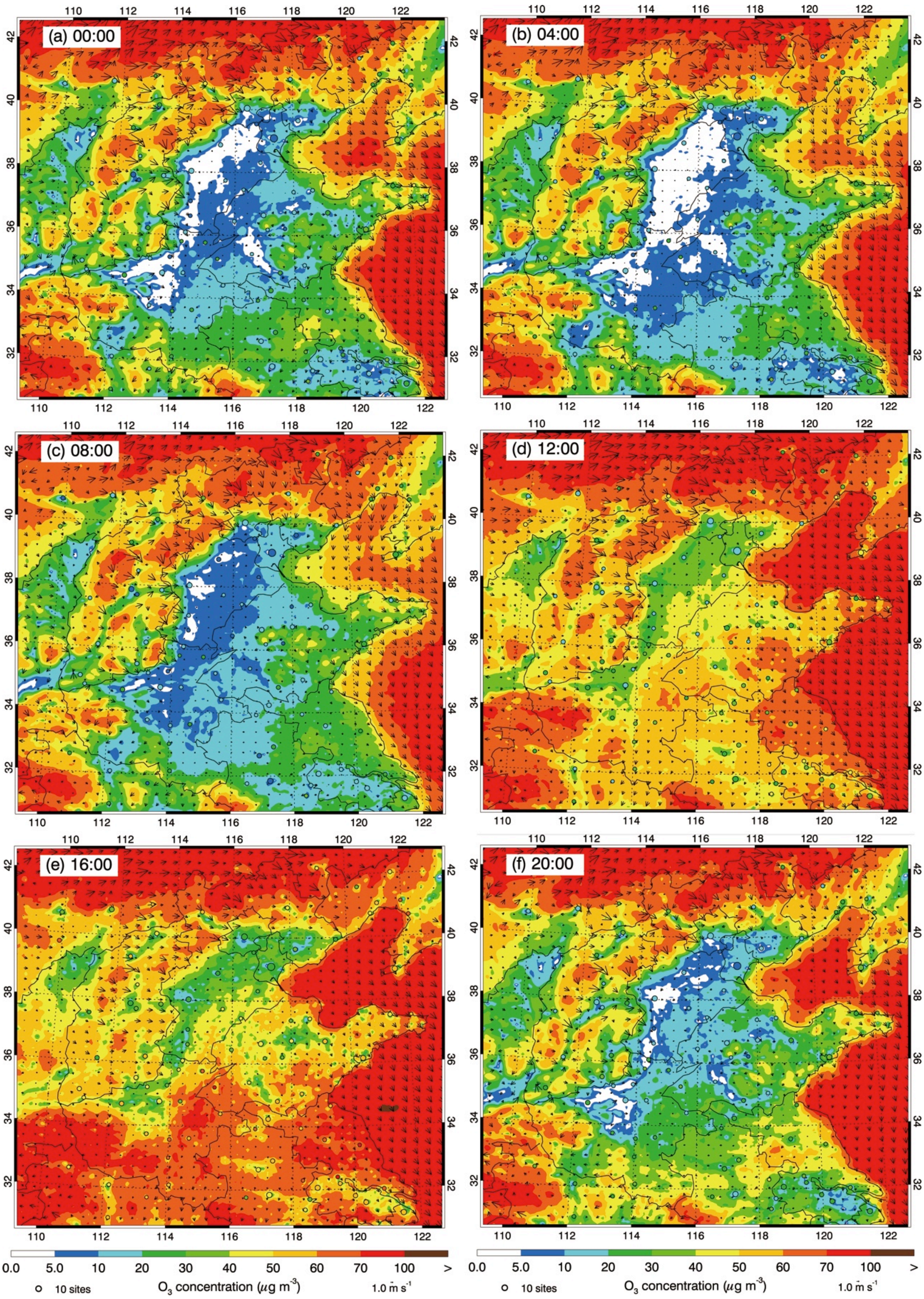

Figure S10 Pattern comparisons of simulated (color contours) vs. observed (colored circles) near-surface mass concentrations of O_3 concentration at (a) 00:00 BJT, (b) 04:00 BJT, (c) 08:00 BJT, (d) 12:00 BJT, (e) 16:00 BJT, and (e) 20:00 BJT averaged from 05 December 2015 to 04 January 2016. The black arrows indicate simulated surface winds.

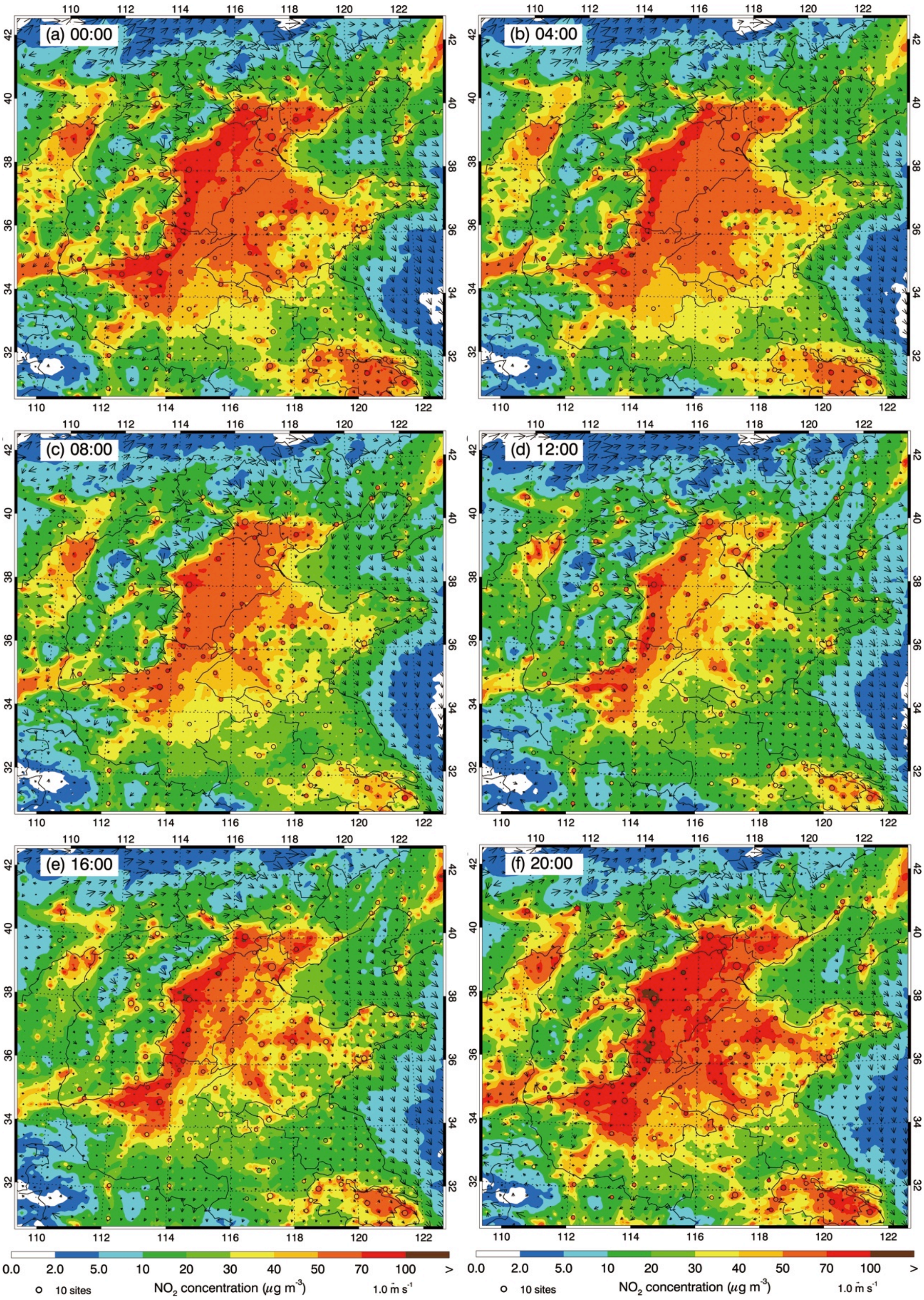

Figure S11 Pattern comparisons of simulated (color contours) vs. observed (colored circles) near-surface mass concentrations of NO_2 concentration at (a) 00:00 BJT, (b) 04:00 BJT, (c) 08:00 BJT, (d) 12:00 BJT, (e) 16:00 BJT, and (e) 20:00 BJT averaged from 05 December 2015 to 04 January 2016. The black arrows indicate simulated surface winds.

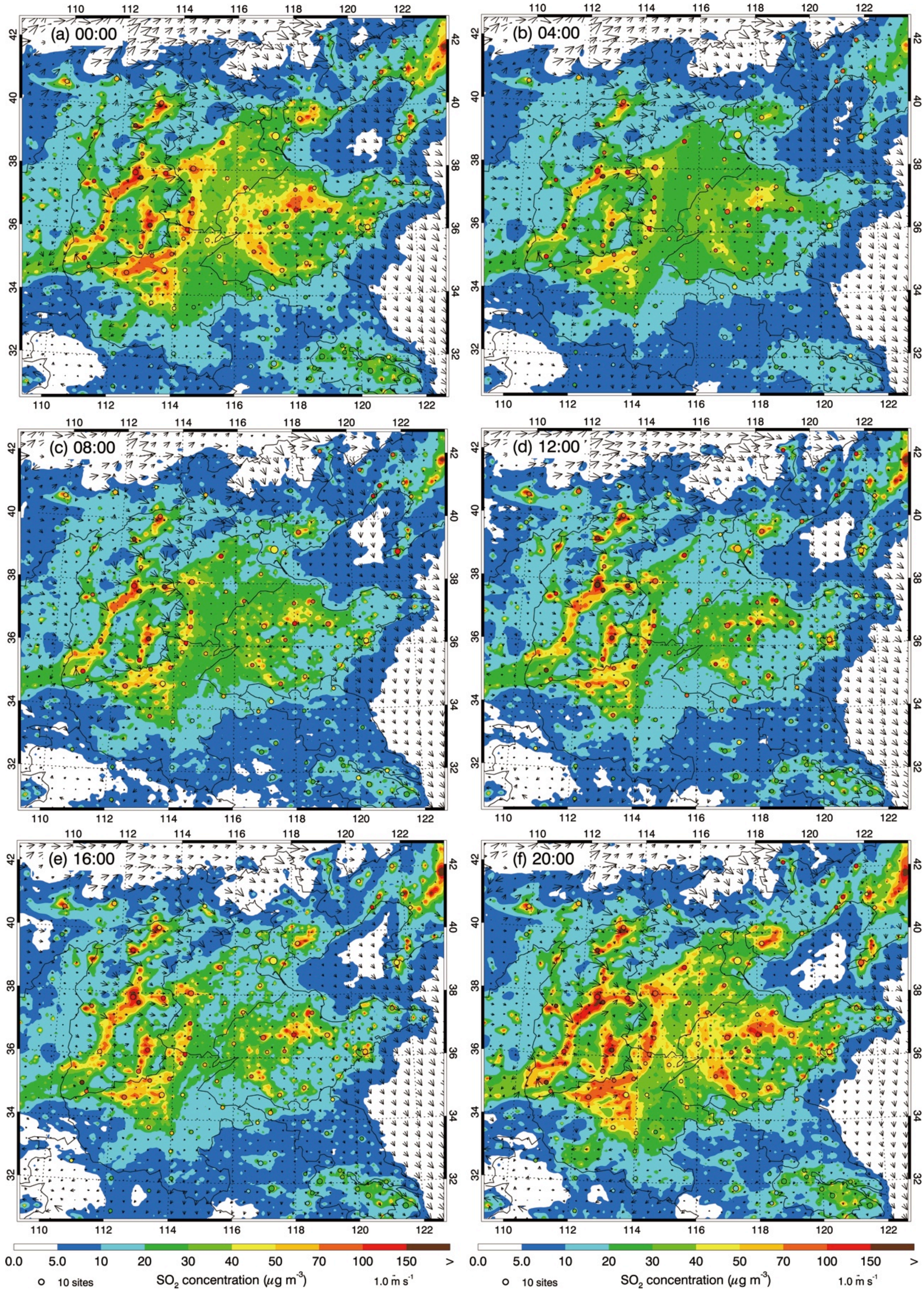

Figure S12 Pattern comparisons of simulated (color contours) vs. observed (colored circles) near-surface mass concentrations of SO_2 concentration at (a) 00:00 BJT, (b) 04:00 BJT, (c) 08:00 BJT, (d) 12:00 BJT, (e) 16:00 BJT, and (e) 20:00 BJT averaged from 05 December 2015 to 04 January 2016. The black arrows indicate simulated surface winds.

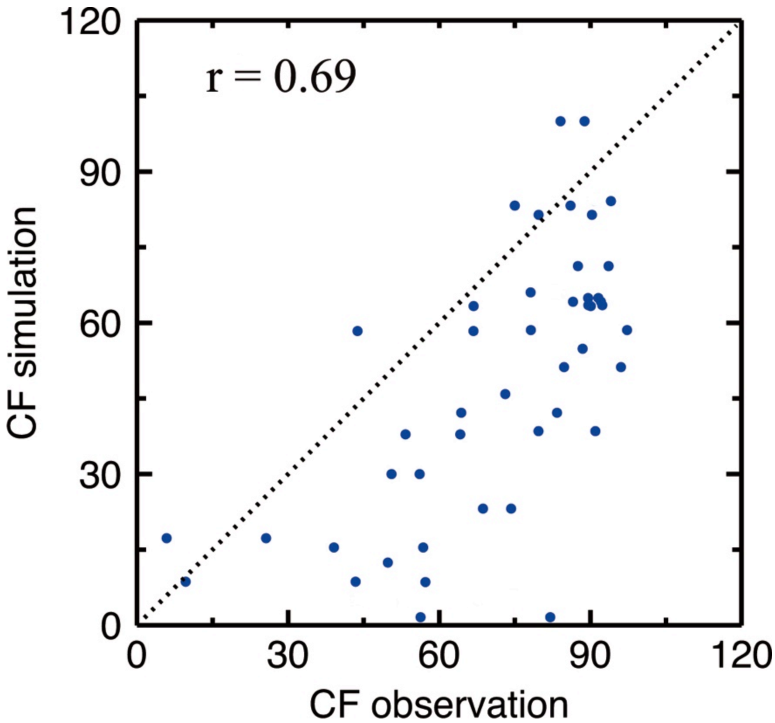

Figure S13 Scatter plot of the MODIS retrieved and simulated daily cloud fraction averaged in the NCP from 05 December 2015 to 31 December 2015.

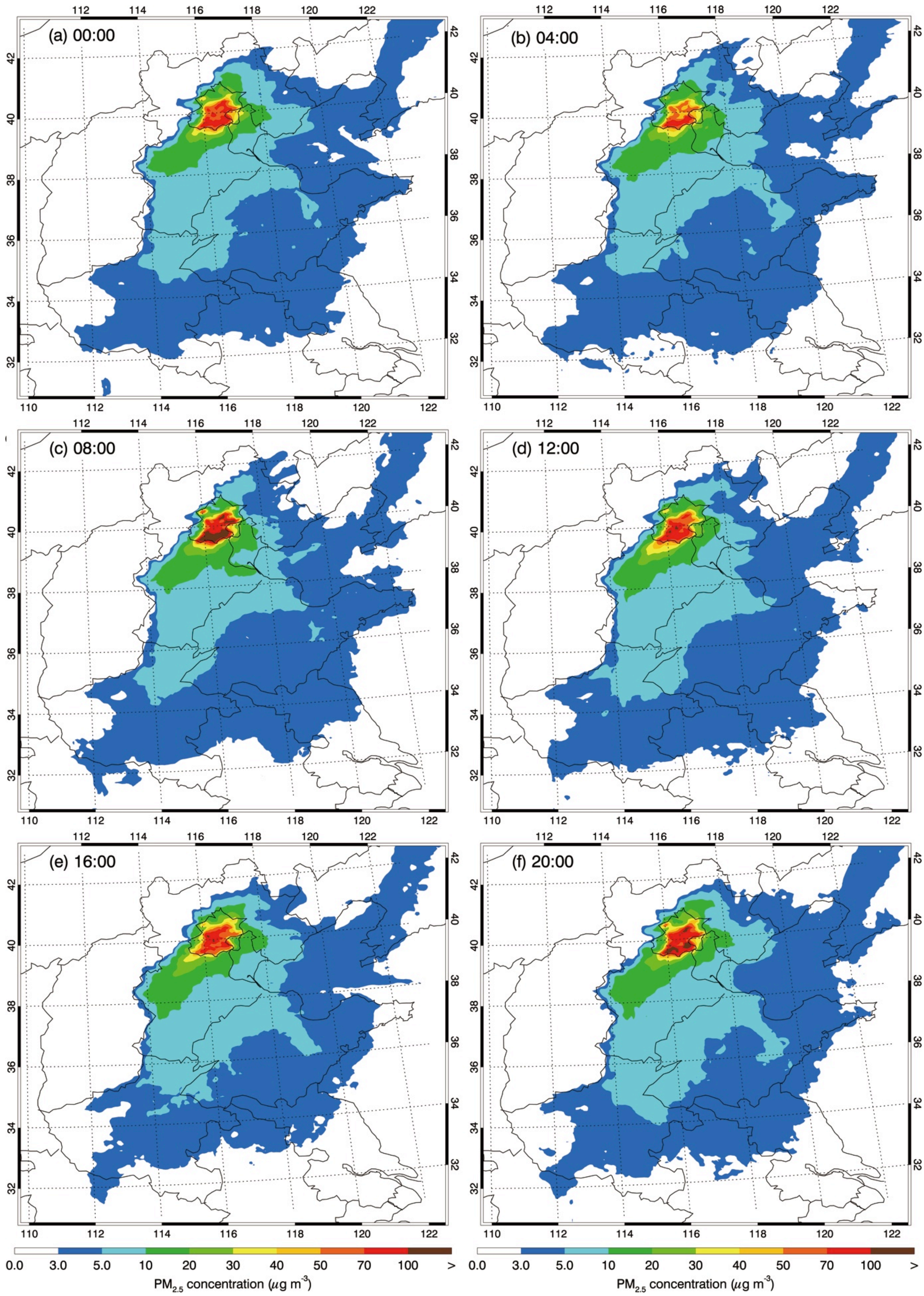

Figure S14 Spatial distribution of average $PM_{2.5}$ contributions from Beijing at (a) 00:00 BJT, (b) 04:00 BJT, (c) 08:00 BJT, (d) 12:00 BJT, (e) 16:00 BJT, and (e) 20:00 BJT averaged from 05 December 2015 to 04 January 2016.

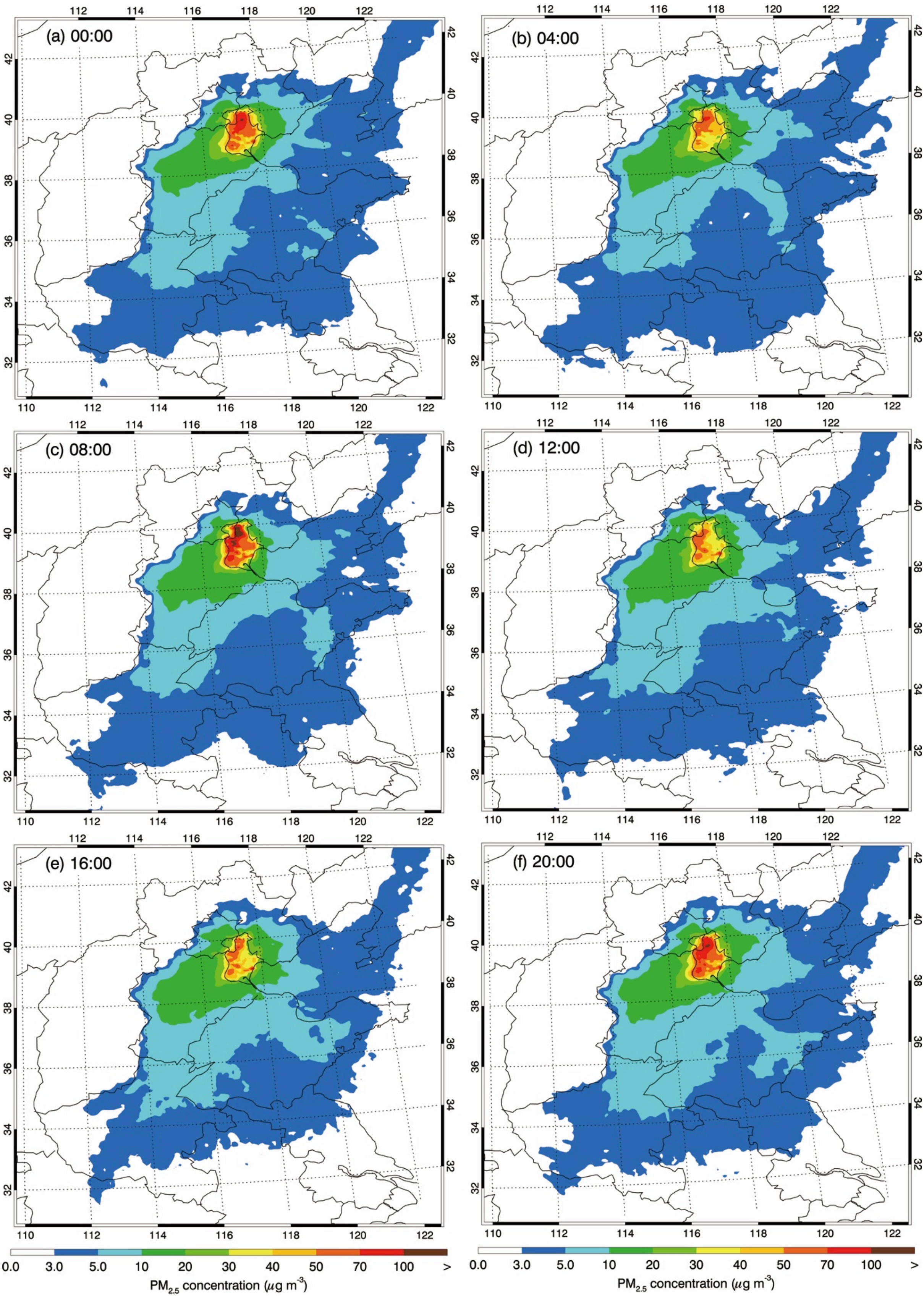

Figure S15 Spatial distribution of average $PM_{2.5}$ contributions from Tianjin at (a) 00:00 BJT, (b) 04:00 BJT, (c) 08:00 BJT, (d) 12:00 BJT, (e) 16:00 BJT, and (e) 20:00 BJT averaged from 05 December 2015 to 04 January 2016.

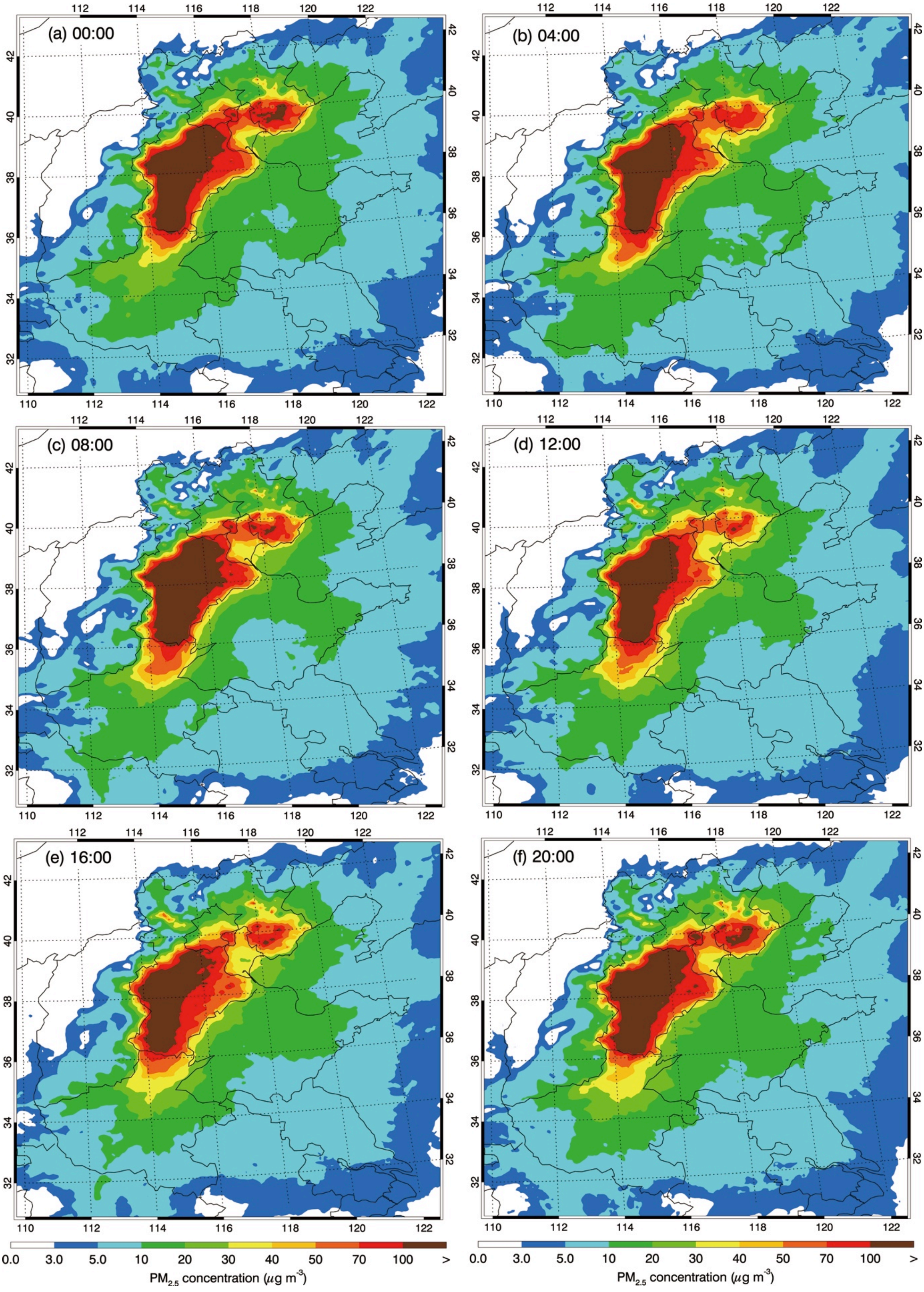

Figure S16 Spatial distribution of average $PM_{2.5}$ contributions from Hebei at (a) 00:00 BJT, (b) 04:00 BJT, (c) 08:00 BJT, (d) 12:00 BJT, (e) 16:00 BJT, and (e) 20:00 BJT averaged from 05 December 2015 to 04 January 2016.

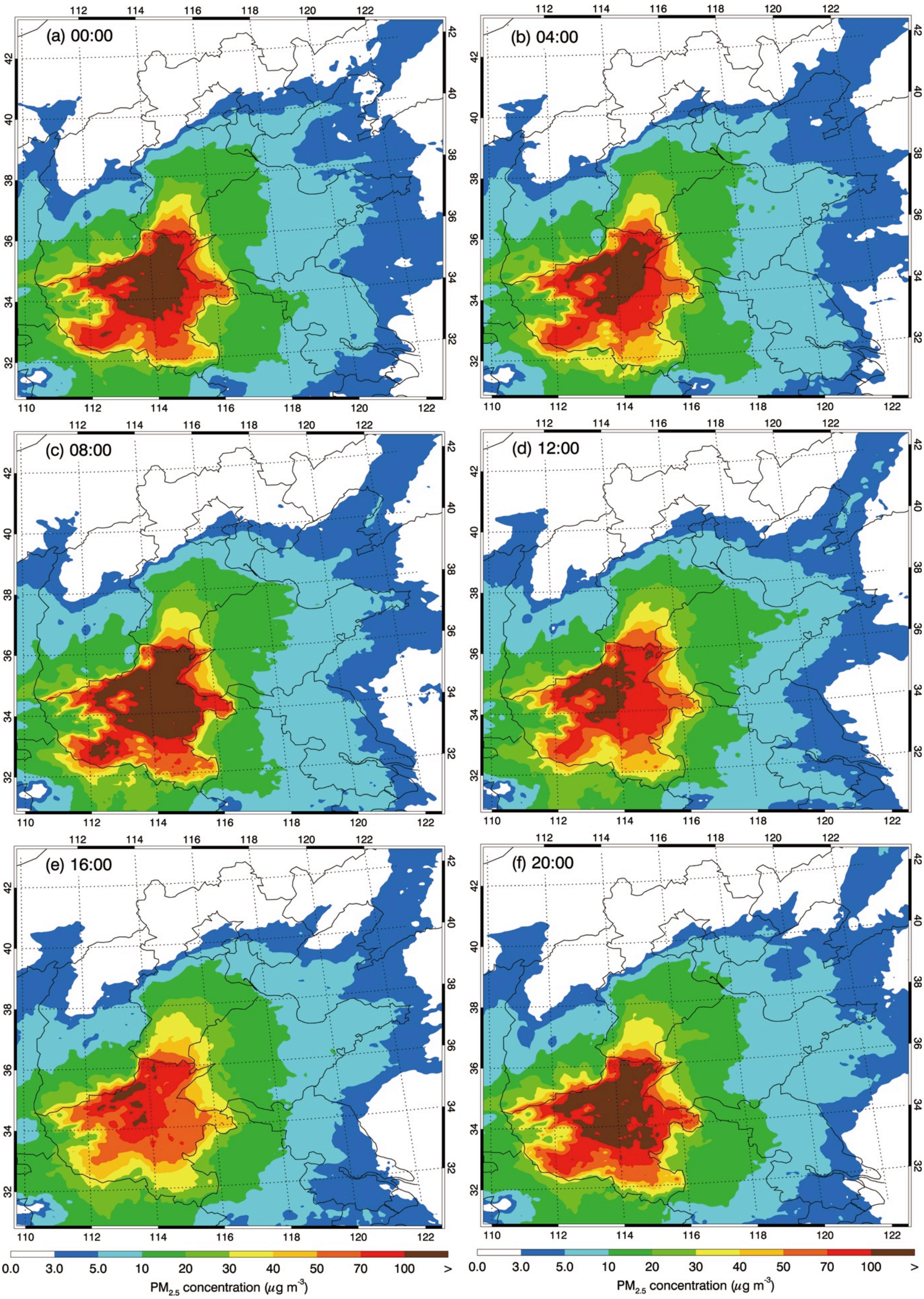

Figure S17 Spatial distribution of average $PM_{2.5}$ contributions from Henan at (a) 00:00 BJT, (b) 04:00 BJT, (c) 08:00 BJT, (d) 12:00 BJT, (e) 16:00 BJT, and (e) 20:00 BJT averaged from 05 December 2015 to 04 January 2016.

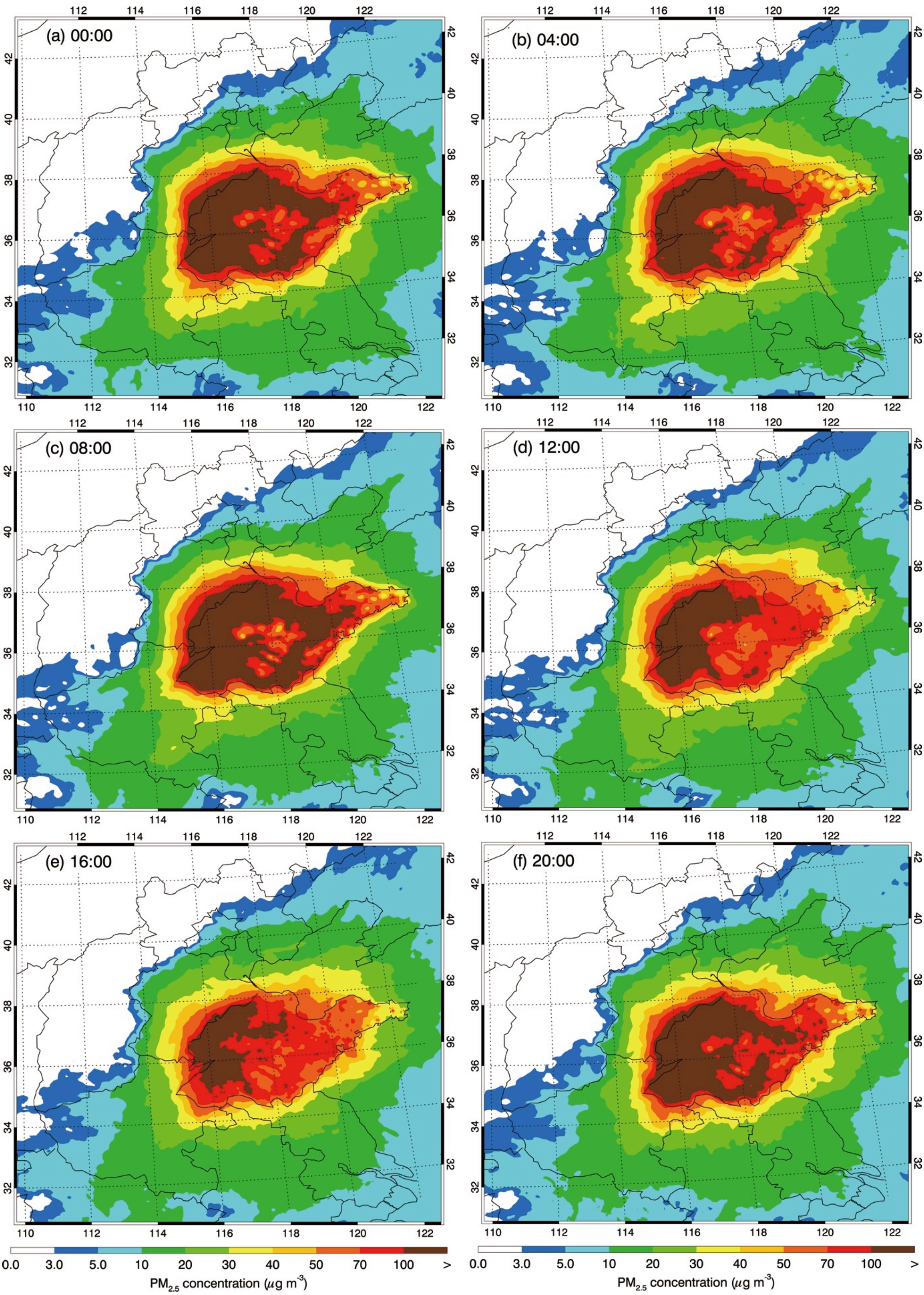

Figure S18 Spatial distribution of average $PM_{2.5}$ contributions from Shandong at (a) 00:00 BJT, (b) 04:00 BJT, (c) 08:00 BJT, (d) 12:00 BJT, (e) 16:00 BJT, and (e) 20:00 BJT averaged from 05 December 2015 to 04 January 2016.

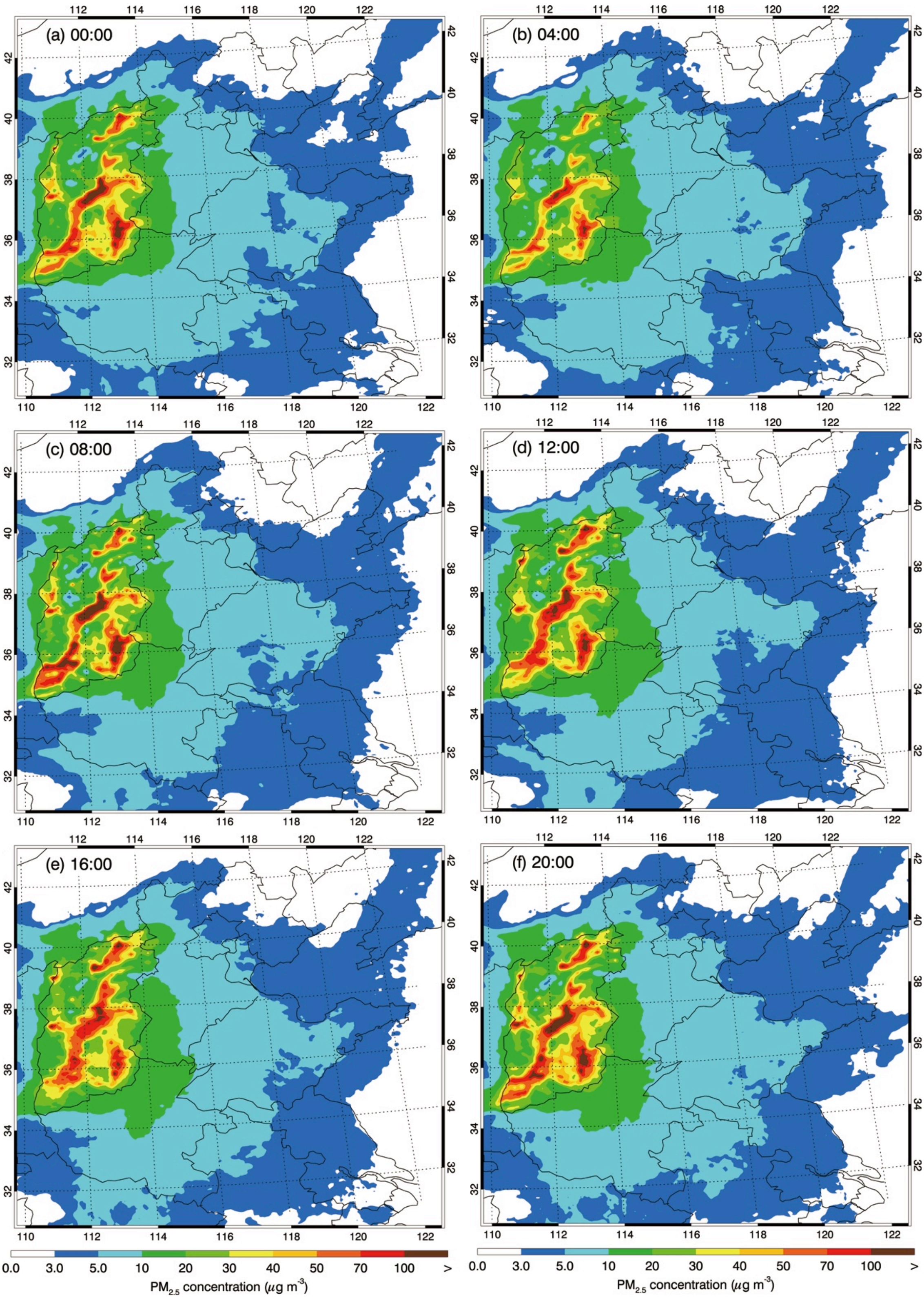

Figure S19 Spatial distribution of average $PM_{2.5}$ contributions from Shanxi at (a) 00:00 BJT, (b) 04:00 BJT, (c) 08:00 BJT, (d) 12:00 BJT, (e) 16:00 BJT, and (e) 20:00 BJT averaged from 05 December 2015 to 04 January 2016.

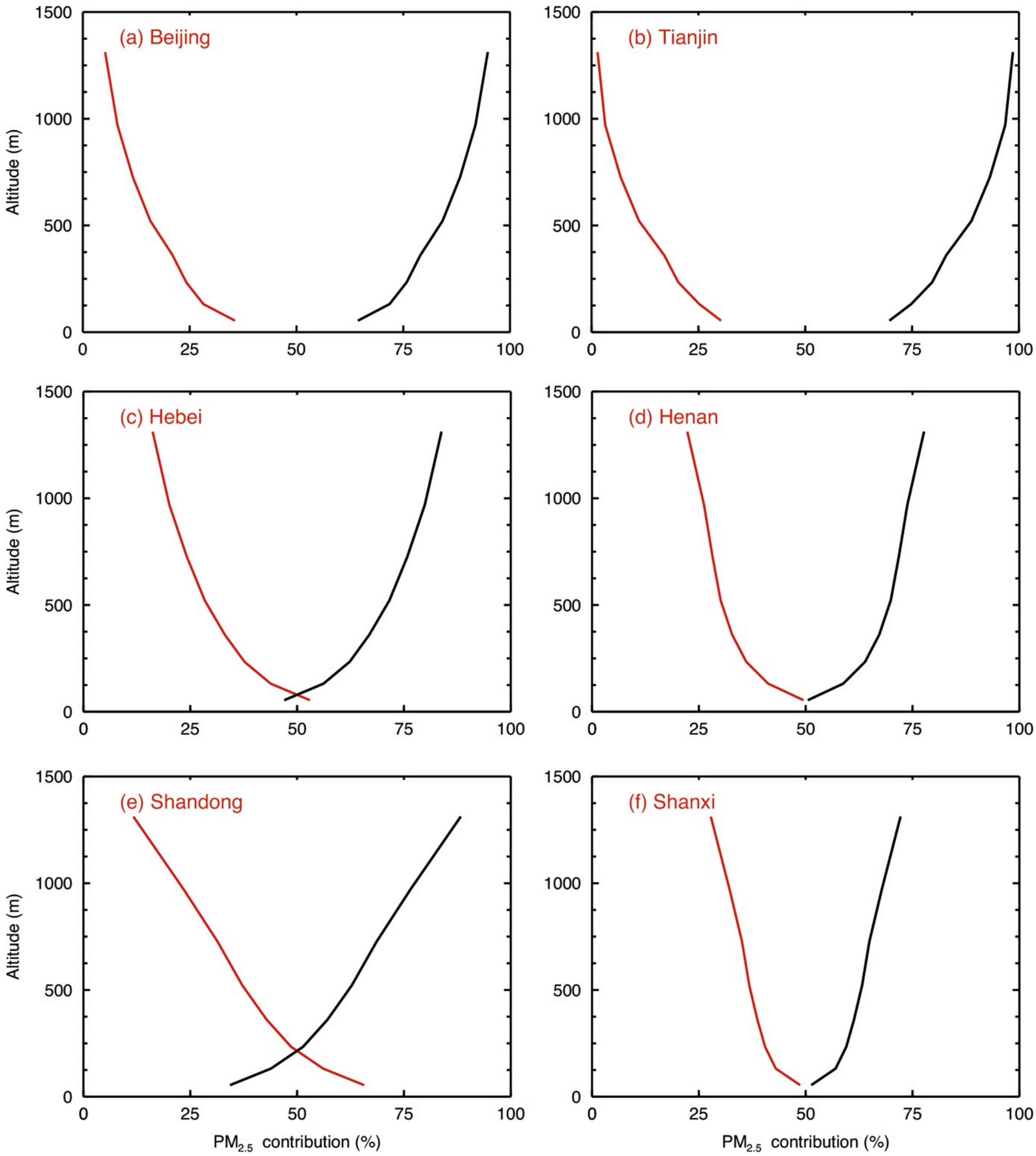

Figure S20 Vertical profiles of average $PM_{2.5}$ contribution from local (red line) and non-local (black line) emissions in (a) Beijing, (b) Tianjin, (c) Hebei, (d) Henan, (e) Shandong, and (f) Shanxi from 05 December 2015 to 04 January 2016.

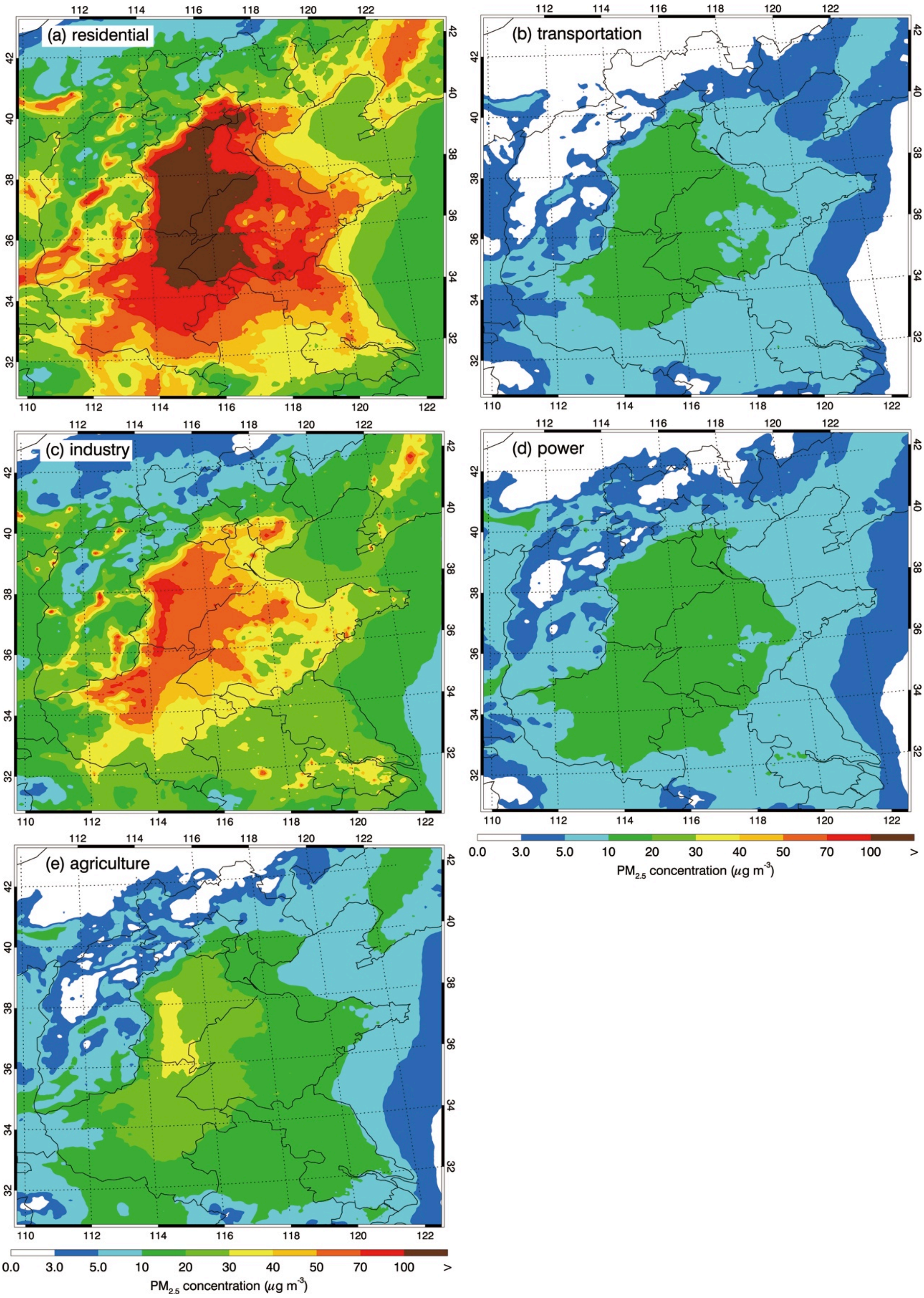

Figure S21 Spatial distribution of average near-surface $PM_{2.5}$ contributions from (a) residential, (b) transportation, (c) industry, (d) power, and (e) agriculture emission sectors from 05 December 2015 to 04 January 2016.

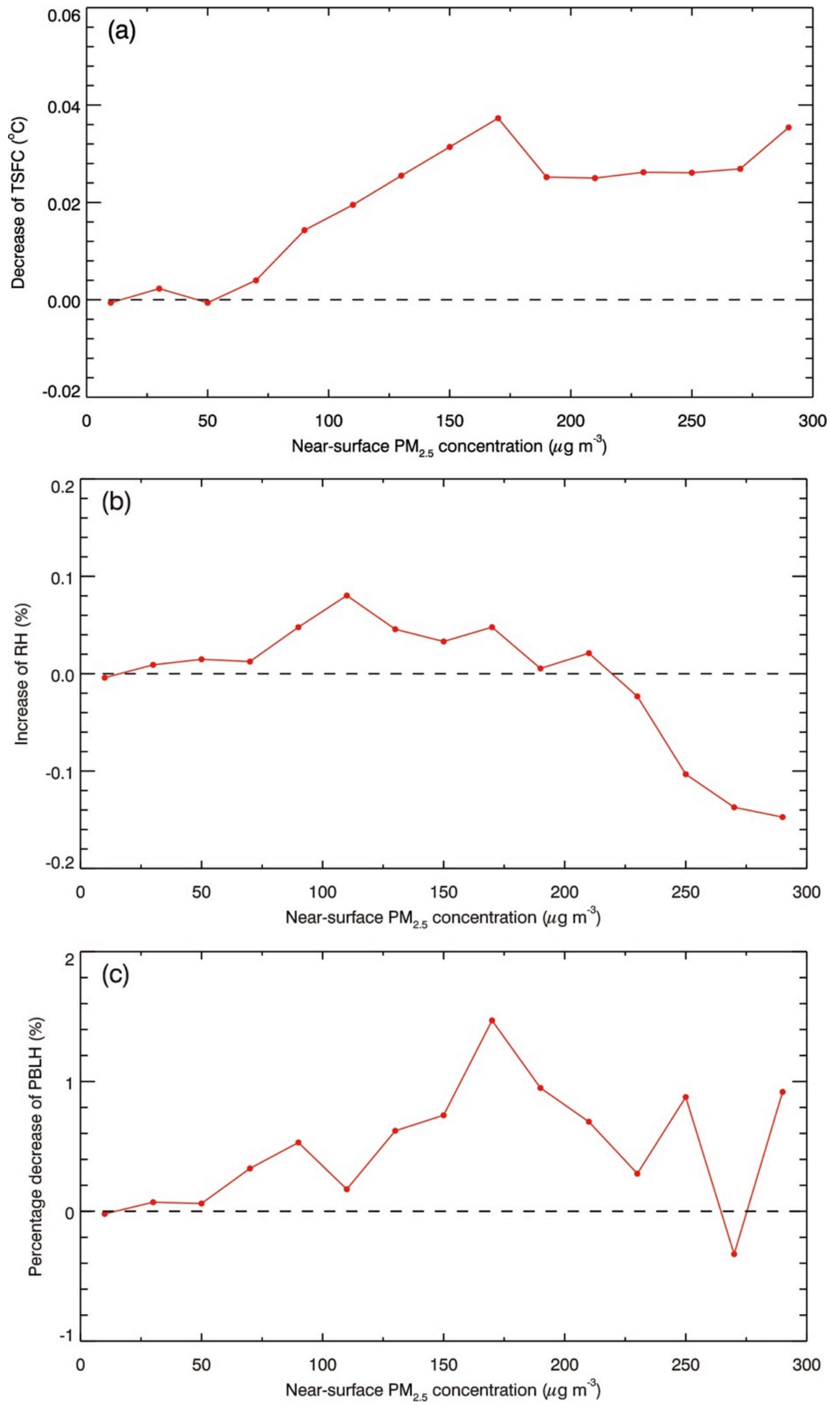

Figure S22 Average (a) decrease of surface temperature (TSFC), (b) increase of relative humidity (RH), and (c) percentage decrease of PBLH caused by the BC transported from the south of 32°N, as a function of the near-surface $PM_{2.5}$ concentration in the NCP during daytime from 05 December 2015 to 04 January 2016.